

Dynamic Fracture Associated with Shallow Dip-Slip Seismic Faulting

Koji Uenishi^{1,*}, Keisho Yamagami¹, Fukutaro Ishida¹, Koji Fujimoto¹

¹ Department of Aeronautics and Astronautics, The University of Tokyo, Tokyo 113-8656 Japan

* Corresponding author: uenishi@mat.t.u-tokyo.ac.jp

Abstract Unlike strike-slip earthquakes, the physical properties of shallow dip-slip quakes remain unexplored because of the insufficient number of near-field seismological recordings and analytical difficulties at the tip of a surface-breaking fault. Here, based on the finite difference technique and dynamic photoelasticity in conjunction with high speed digital cinematography, we numerically and experimentally simulate the source dynamics of dip-slip faulting. Our two-dimensional model may contain a flat fault plane (interface) dipping either vertically or at some angle in a monolithic linear elastic medium. We record the evolution of wave field related to the crack-like rupture along this fault. The observations suggest if the fault rupture, initiated at some depth, arrests just below or reaches the free surface, four Rayleigh-type waves are generated: two propagating along the free surface into the opposite directions to the far field, the other two moving back along the fractured interface downwards into depth. These downward interface waves may largely control the stopping phase of the dynamic rupture. In the case of an inclined fault plane, the interface and Rayleigh waves interact with each other and a shear wave carrying concentrated kinematic energy (corner wave) is induced to generate enormously strong particle motions in the hanging wall.

Keywords Earthquake dynamics, Earthquake ground motions, Fracture dynamics, Experimental mechanics, Computational seismology

1. Introduction

After the reasonable agreement between the theoretical and observational near-field seismograms related to the 1966 strike-slip Parkfield, California, earthquake [1], the techniques to evaluate the near-field generated by strike-slip faulting have become remarkably refined. At present it is common to invert seismological recordings for estimating fault slip distribution, rupture history and their effects for large, shallow strike-slip earthquakes [1–4]. However, the situation is different for shallow dip-slip earthquakes since only few seismic events of this type have been well recorded in the near-field and the mechanical characteristics have not been fully clarified owing to analytical difficulties at the tip of a surface-breaking fault [4–15]. Hazard risk due to such dip-slip earthquakes may be higher in the tectonically compressive regions like Los Angeles, Japan and Taiwan, Central and South America, and in extensional regimes such as the Mediterranean and the Great Basin of Nevada, Utah, and Idaho [5], and an extensive effort has been made to model dip-slip events and the strong motion (particle motion) generated by them [4–15]. Earlier study of shallow dip-slip faulting is based on kinematical models, using the Cagniard-de Hoop [12] or a numerical spectral method [13]. But the analysis becomes very sophisticated and often it does not work correctly, because of analytical singularities, when the fault rupture reaches the free surface. Nevertheless, the previous works posed questions regarding the effect of the free surface near the shallow dipping fault, which require careful study [4].

One noteworthy observation in shallow dip-slip earthquakes is the asymmetric ground motion in the vicinity of the fault: Generally, strong motion is much larger in the hanging wall than in the footwall. For example, the 1971 San Fernando and the 1994 Northridge earthquakes caused systematically severer damage or larger ground motion on the hanging wall [5]. The more recent earthquakes, the 1999 Chi-Chi in Taiwan [6, 7] and the 2004 Niigata-ken Chuetsu [16] and 2008 Iwate-Miyagi Inland [17] in Japan, seem to support this viewpoint. This observed effect is considered to be caused by the strong disturbance in the proximity of the propagating rupture front (rupture front wave) [4], the trapped wave in the hanging wall [5], or the asymmetric mass distributions on each wall and the

normal stress acting perpendicular to the fault surface [5, 7–9]. However, the dynamic properties of shallow dip-slip faulting are not fully understood yet.

Here, in order to give a possible physical explanation of the abovementioned observation, we numerically and experimentally study rupture (fracture) dynamics of a dip-slip fault (interface) situated in a two-dimensional, monolithic linear elastic medium. We employ the finite difference technique for numerical simulations on a PC basis, and in a series of experiments, we initiate rupture in the birefringent linear elastic material using a Q-switched Nd:YAG laser system or a projectile launched by a gun. We record the time-dependent evolution of the wave field induced by the crack-like rupture along the fault, and also monitor the particle motions on the free surface of the model.

2. Geometry and setting

Our model contains a fault plane dipping either 90° (vertical) or 45° (nonvertical case) (Fig. 1) and in each case, the initial static shear stresses acting on the fault plane are set to be equal: For the vertical case (Fig. 1a), remote shear loading which increases linearly with depth is assigned; In the nonvertical case (Fig. 1b), compressive normal stress increasing with depth is given so that linearly increasing static shear stress acts on the fault plane (Fig. 1b). Using the finite difference technique [18], we study the seismic wave field (isochromatic fringe patterns) produced by rupture of this straight fault and try to gain insight into the free surface effect on dip-slip faulting.

As we consider the problem in the framework of linear elasticity, we may assume, without loss of generality, the longitudinal (P) wave speed c_P in the medium is 1. If Poisson's ratio is 0.25, then the shear (S) wave speed c_S becomes $1/\sqrt{3}$ (~ 0.58) and the Rayleigh (R) wave speed c_R is about 0.53. We use the orthogonal 201 times 201 grid points and calculate displacements at each grid point with the second order accuracy. The uniform spacing between each orthogonal grid is 0.05, and the time step is also constant to be 0.025. We further assume the energy absorbing boundary conditions to the outer boundaries except for the upper free surface where the vertical normal and the tangential shear stresses are always zero.

We simulate three different situations: finite fault that ruptures only at depth (Fig. 2); fault rupture (interface crack) starting at depth and arrested well below the free surface (Fig. 3); and fault rupture initiated at depth and reaching the free surface (Fig. 4). By showing the time-dependent dynamic (maximum in-plane shear) stress field, we suggest that the magnitudes of the stresses induced in the

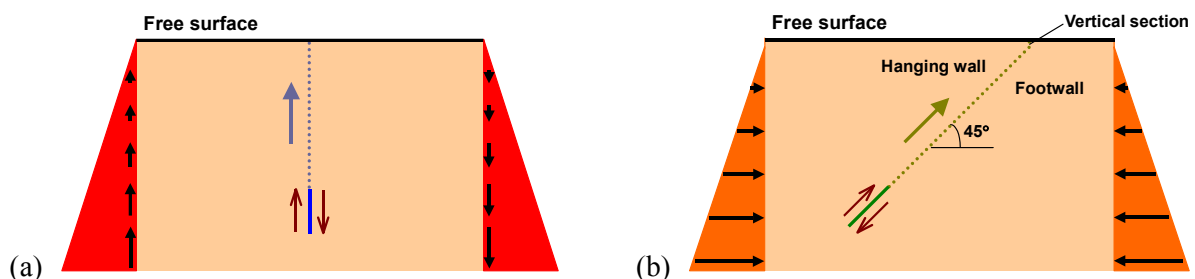


Figure 1. Schematic diagram of the geometry of the dip-slip fault model. For both (a) vertical and (b) nonvertical (45° dipping) situations, we assume a monolithic, linear elastic medium. The fault rupture (interface crack) starts at the bottom and in later simulations it propagates towards the free surface. While the geometrical symmetry is preserved in (a), the symmetry between the free surface and the two sides of the fault (hanging wall and footwall) is broken in (b).

hanging wall and in the footwall may become completely dissimilar for the three cases. Note, in all numerical simulations, we assume crack-like rupture, i.e., once a fault segment is ruptured, the accumulated static shear stress on that segment is released and that section of the fault remains broken without being healed. As shown in Fig. 1, fault slip (displacement discontinuity) is oriented so that the fault behaves as a thrust one, but the results shown below are valid also for normal dip-slip faulting. In the following, snapshots of the isochromatic fringe patterns, i.e., contours of the (dynamic) maximum in-plane shear stress (τ_{\max}), are exhibited where the fringe order is proportional to τ_{\max} (≥ 0) and all types of elastic waves may be displayed.

3. Numerical case studies

3.1. Finite fault buried at depth

Figure 2 shows the dynamic rupture-induced stress field for the case of a finite dip-slip fault located at depth (length $L = 0.05$, depth $h = 2$ and $L = 0.05\sqrt{2}$, $h = \sqrt{2}$ for the vertical and nonvertical cases, respectively). This problem is rather classical in seismology: The entire (short) fault segment breaks instantaneously at time $t = 0$ to radiate body waves. At time $t = 1.5$, we recognize weak shear waves radiated from the hypocenter (identified as S in the figure). In the geometrically symmetrical case (Fig. 2a), at $t = 3.9$, clear but weak surface reflected *SS* wave and two Rayleigh surface pulses (R) are visible. We also find weak *PS* waves, the *P* waves diffracted by the free surface and converted into *S* waves, but the *P* wave front propagating from the hypocenter is invisibly weak. These *PS* waves interact with the outgoing *S* waves, but their effects seem, again, negligible. At later stages ($t = 6.3$ and 8.7), both surface pulses *R* follow the *S* waves and propagate into the far-field (without decay in these two-dimensional simulations), but the reflected shear wave *SS* attenuates upon propagation and its interaction with the seismic source (hypocenter), now showing static stress singularities, is very small. Similar discussion holds in the asymmetrical case (Fig. 2b) except that here Rayleigh pulse (R_h) and shear wave (S_h) in the hanging wall are stronger than those (R_f and S_f) in the footwall. It is important to note that in seismology an approximate (kinematic) approach, stacking the finite fault segments and rupturing these segments sequentially, is usually employed to inversely obtain a progressive fault rupture related to an earthquake (seismograms). However, from dynamics point of view this approach may not be valid because, as we see below, the wave field generated in the finite fault segments approach (Fig. 2) has a characteristic radiation pattern very different from the one associated with the continuously rupturing fault (Figs. 3 and 4). This situation is akin to blasting simulations of a progressively detonating column charge: The characteristic dynamic wave patterns in the approximate approach that is based on stacking spherical charges and detonating these charges sequentially are very dissimilar compared with the radiation patterns of continuously exploding charge [19, 20].

3.2. Fault rupture starting at depth and arresting well below the free surface

In Fig. 3, the fault rupture is initiated at depth ($h = 2$ and $\sqrt{2}$ for Figs. 3a and 3b, respectively), propagated upwards but suddenly arrested well below the free surface. At time $t = 0$, fracture starts moving along the prescribed fault plane with a constant speed c , and after a certain time $t = L/V$ it arrests, leaving a final rupture zone of length $L = 1$. For this crack-like fault model, we assume the constant rupture speed is in the subsonic range, $0.4 c_P$ ($\sim 0.7 c_S$; smaller than the Rayleigh wave speed c_R). The noteworthy phenomenon observed here is the strong rupture front wave ($t = 1.5$). In the vertical case (Fig. 3a), the problem is still geometrically symmetrical and the induced particle motions are symmetrical with respect to the rupturing fault plane: Upon arrest, a relatively strong shear wave (S_1) is radiated from the upper tip of the ruptured fault plane (interface) ($t = 3.9$) and

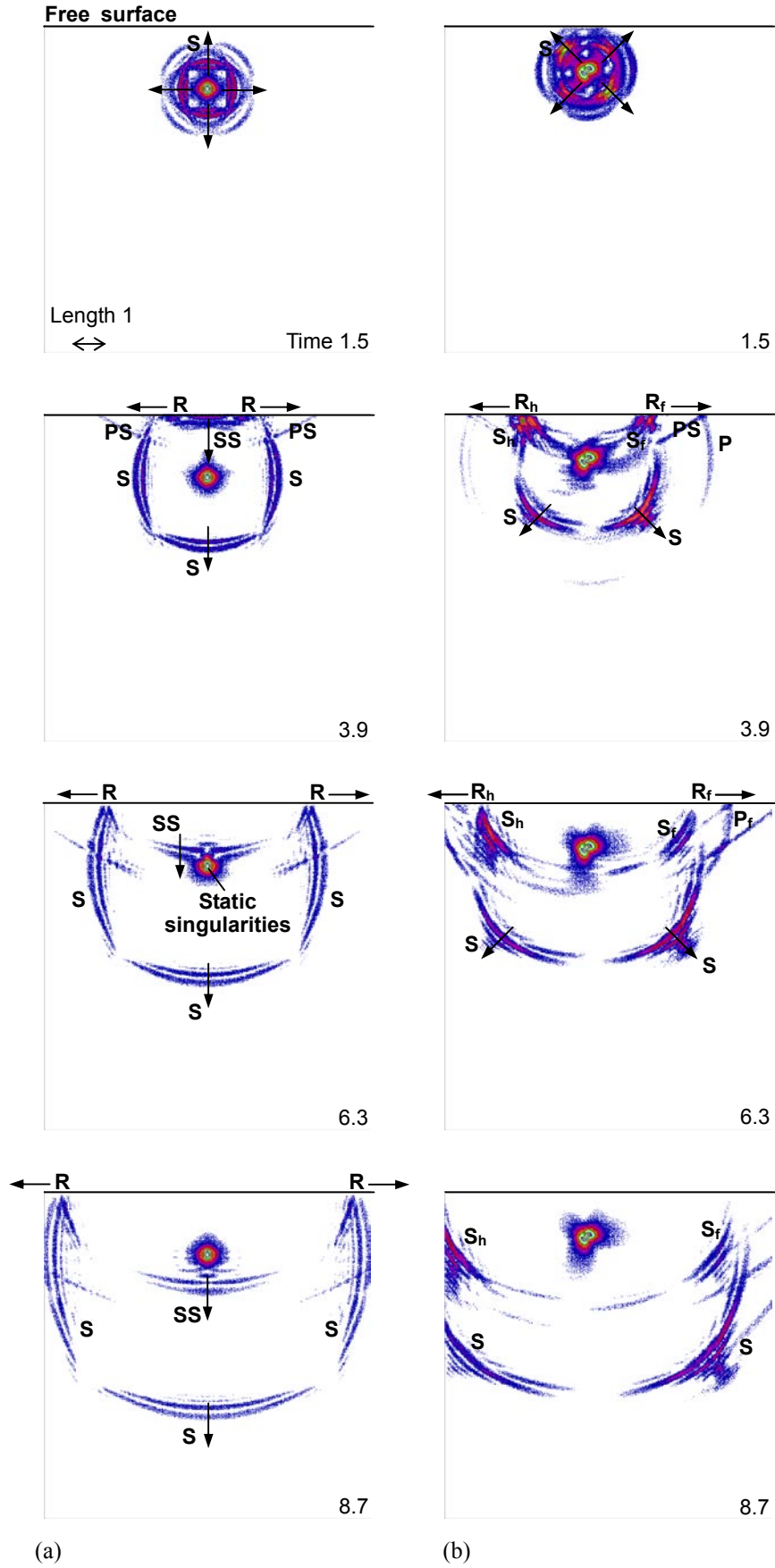


Figure 2.

interacts with the free surface. The reflected shear wave (SS) and another shear (S_2) wave generated by the stopping phase of the rupture process interact with the ruptured interface but their influence on the interface seems relatively small. Rayleigh pulses propagating along the free surface are much stronger than those in Fig. 2a. When the fault plane is nonvertical (Fig. 3b), the geometrical symmetry is totally broken: The induced stress is much larger in the footwall than in the hanging wall, with a much stronger shear S_f wave recognizable in the footwall. It is contrary to the previous and the following observations (Figs. 2b and 4b) where the dynamic disturbances are stronger in the hanging wall than in the footwall, and it may be due to the strong rupture front wave that is diffracted at the upper tip of the ruptured interface and flows into the footwall across the unbroken (extended) section of the fault plane.

3.3. Fault rupture approaching the free surface from bottom

The wave field where the fault breaks the free surface is shown in Fig. 4. As in the previous case (Fig. 3), the crack-like rupture, starting at $t = 0$, propagates along the fault plane with a constant speed $c = 0.4 c_P$ for a length $L = 2$ until it surfaces. In both vertical and nonvertical cases, when the rupture front approaches the free surface, four Rayleigh-type pulses are generated: two propagating along the free surface into the opposite directions to the far-field (labeled as R or R_h , R_f), the other two moving back along the ruptured interface downwards into depth (I). This downward surface-type pulse can be observed also in the numerical simulations of borehole blasting in a rock mass where the explosive charge is detonated at the bottom and a detonation front moves along an explosive column toward the free surface (bottom-to-top blasting); Rayleigh pulses are generated when the detonation front reaches the surface and they may move downwards along the explosive column [19, 20]. If the fault is vertical and geometrically symmetrical (Fig. 4a), the downward interface pulses may largely control the stopping phase of the dynamic rupture on the fault. If the fault is nonvertical and asymmetrical (Fig. 4b), the downward interface pulse and the outward-moving surface pulse (R_h) interact with each other to induce a specific shear wave, corner wave (C), in the hanging wall. This corner wave carries concentrated wave energy and generates strong particle motions in the hanging wall. In the footwall, on the contrary, the weaker surface pulse (R_f) dominates the ground (free surface) motion and the interaction of this surface pulse with the interface pulse moving in the opposite direction (I) is also small. Thus, the asymmetric ground motion, abovementioned and often observed in shallow dip-slip earthquakes, may be caused. The P and S waves generated in the footwall upon fault surfacing (P_f , S_f) is also relatively strong, but they are much weaker than the corner wave in the hanging wall. The generation of the interface pulse and the corner wave has not been well recognized so far, partly because these waves may not be expected for a fault fracturing only at depth (Figs. 2 and 3), but we should note that similar rupture pattern (downwards rupture after initial upward one) has been reported for the rupture development related to the 2011 off the Pacific coast of Tohoku, Japan, earthquake [21]. In the simulation of the surfacing nonvertical fault, the shallowest part (length 0.15, i.e., three times the grid spacing; see Fig. 1b) is assumed vertical so that we can numerically treat the corner effect appropriately in the framework of the finite difference method: This geometry is selected so as to avoid the problems related to analytical singularities. However, further computations may indicate that qualitatively same phenomena can be observed without this short vertical section, i.e., even when the nonvertical fault rupture stops just below the free surface (at a very shallow depth of 0.15). However, the amplitudes of the induced surface, interface pulses and the corner waves become smaller.

Figure 2 (continued). Snapshots of the dynamic stress field (isochromatic fringe patterns) associated with the rupture of the (a) vertical and (b) nonvertical finite dip-slip seismic sources at depth. The fringe order is proportional to the magnitude of the maximum in-plane shear stress (τ_{\max}). Rupture is initiated at time $t = 0$. Weak Rayleigh surface pulses as well as the waves reflected at the free surface can be recognized.

4. Preliminary experimental results

Next, in order to try to confirm the numerical results, we perform laboratory photoelastic fracture experiments using a birefringent linear elastic material as well as a Q-switched Nd:YAG laser system or a projectile launched by a gun. We prepare a pre-cut interface in a polyurethane plate (50 mm × 25 mm × 12 mm), which is essentially under no static stresses. Dynamic fracture may be induced upon initiation of irradiation of laser pulses or incidence of a projectile (at a speed of 55.5 m/s) and propagated along the interface that is vertical or inclined at an angle of 45 degrees. We record the development of dynamic wave field with a high speed digital video camera system at a frame rate of 100,000 fps (e.g., Fig. 5 for incidence of a projectile), and at the same time, we monitor the particle motions on the free surface using a laser displacement meter (at positions 6 mm away from the surface-breaking point). The observations show that the experimental dynamic isochromatic fringe patterns are similar to the wave patterns generated by the numerical simulations, and if the inclined fault rupture reaches the free surface, the maximum vertical surface displacement on the hanging wall is about 4.6 times as large as that on the footwall (Fig. 6). On the contrary, as is expected from Fig. 3, when the fracture of the interface is arrested well below the free surface (arrested depth equal to a half of the plate height), the vertical motion on the footwall becomes about 1.2 times as large as that on the hanging wall.

5. Conclusions

We have studied the dynamic model of the seismic wave field radiated by rupture of a dip-slip fault located near Earth's free surface. The results of the numerical simulations and preliminary experiments suggest that the dynamic stresses and surface particle motions in the hanging wall, induced by nonvertical dip-slip faulting, may become larger or smaller than those in the footwall, depending on the depth of the arresting point of the fault rupture. We have also indicated that if the fault rupture starting at some depth approaches the free surface, four Rayleigh-type pulses (waves) may be produced: two moving along the free surface and the other two propagating back downwards along the ruptured interface. The downward interface pulses may considerably affect the stopping phase of the dynamic fracture process, and indeed, they might have governed the seismic rupture associated with the 2011 off the Pacific coast of Tohoku earthquake in Japan. If the fault plane is inclined, the interface pulse may interact with the Rayleigh pulse to generate a strong corner shear wave in the hanging wall. In the footwall, the interaction between the Rayleigh and interface waves is much smaller and the ground (free surface) motion is dominated simply by a weaker Rayleigh wave propagating along the free surface. The existence of downward interface waves and corner wave, which is not expected from a conventional seismological analyses where a fault ruptures only at depth, may play a crucial role in understanding the effect of the geometrical asymmetry on the strong motion induced by shallow dip-slip faulting. As stated above, the seismological recordings of recent earthquakes seem to support this idea, and there is certainly a need for careful consideration of dynamic fracture process along a shallow dip-slip fault plane. Although the model employed here is simple, they may provide a dynamic physical explanation of the observations associated with shallow dip-slip earthquakes.

Figure 3 (continued). The τ_{\max} stress field induced by the (a) vertical and (b) nonvertical crack-like dip-slip faulting. Rupture starts at depth at time $t = 0$ and moves upward at a constant speed to suddenly arrest well below the free surface. The rupture propagation speed is assumed to be below the Rayleigh wave speed. In both cases, the rupture front wave, a strong disturbance in the proximity of the propagating rupture front, can be identified. In (b), the amplitude of the shear wave is larger in the footwall than in the hanging wall, because much of the energy carried by the rupture front wave in the hanging wall is diffracted at the tip of the broken fault segment and flows into the footwall.

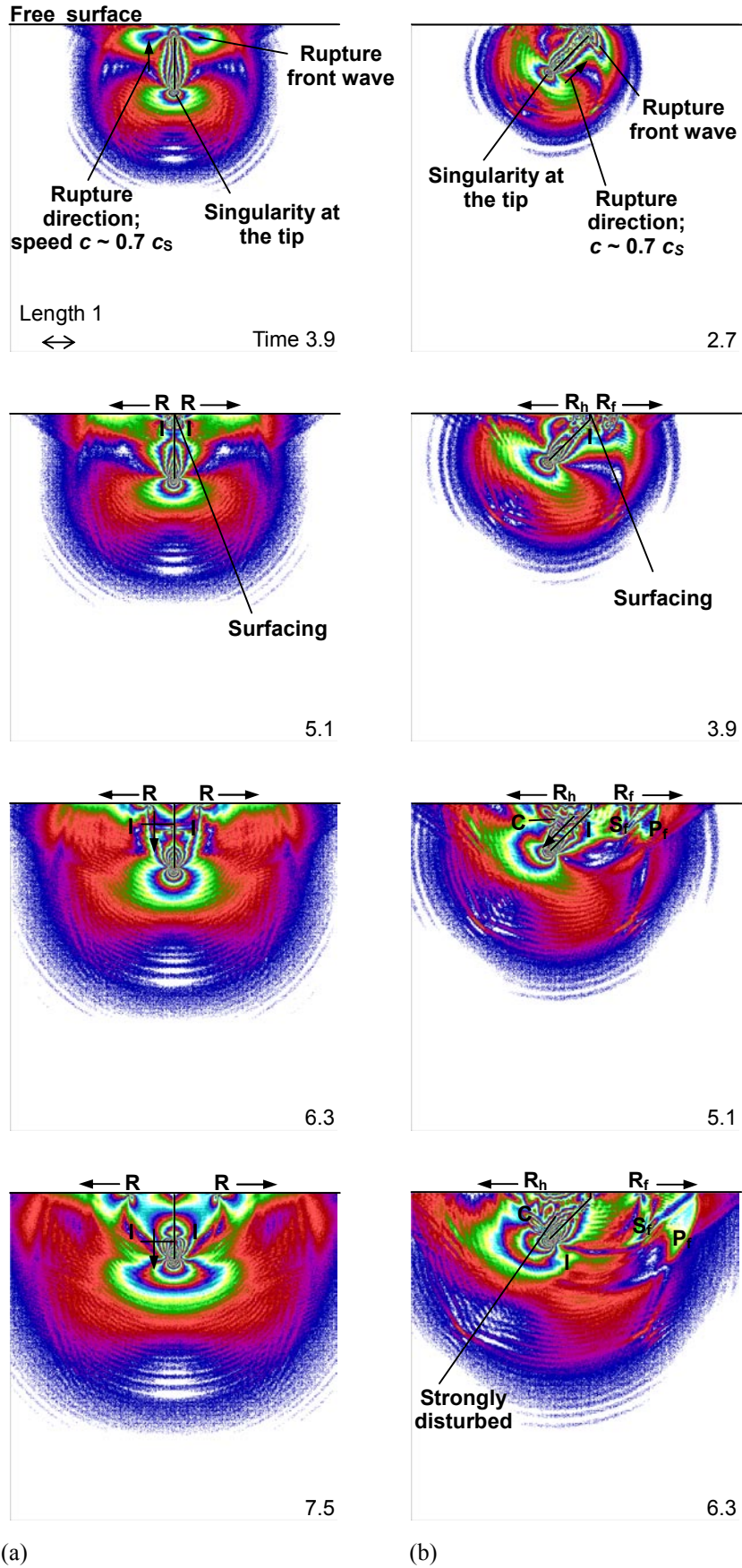


Figure 4.

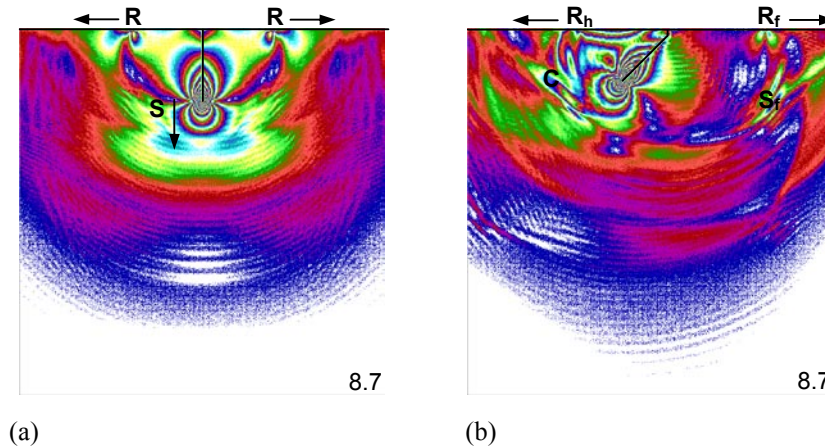


Figure 4 (continued). The sequence of snapshots of the τ_{\max} stress field induced by the (a) vertical and (b) nonvertical dip-slip faulting. As in Fig. 3, the rupture, initiated at depth at $t = 0$, propagates upwards but now it breaks the free surface. In (a), upon fault surfacing, four surface-types waves are generated: The Rayleigh pulses (waves) (marked as R) move along the free surface into the far-field and the interface pulses (I) propagate downwards along the ruptured fault surfaces. At a later stage ($t = 8.7$), the interface pulses merge into a shear wave. In (b), the wave energy trapped in the hanging wall is identifiable as a Rayleigh pulse R_h and the corner wave C. Strong dynamic disturbance may be found in the hanging wall behind the corner wave while in the footwall the induced stresses are relatively small.

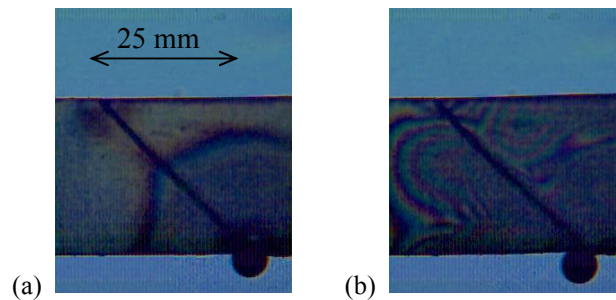


Figure 5. The experimentally obtained snapshots of isochromatic fringe patterns showing the typical dynamic wave field induced by fracture of an interface inclined at an angle of 45 degrees to the free surface. The photographs are taken at (a) 40 and (b) 280 μs after the incidence of the projectile, respectively.

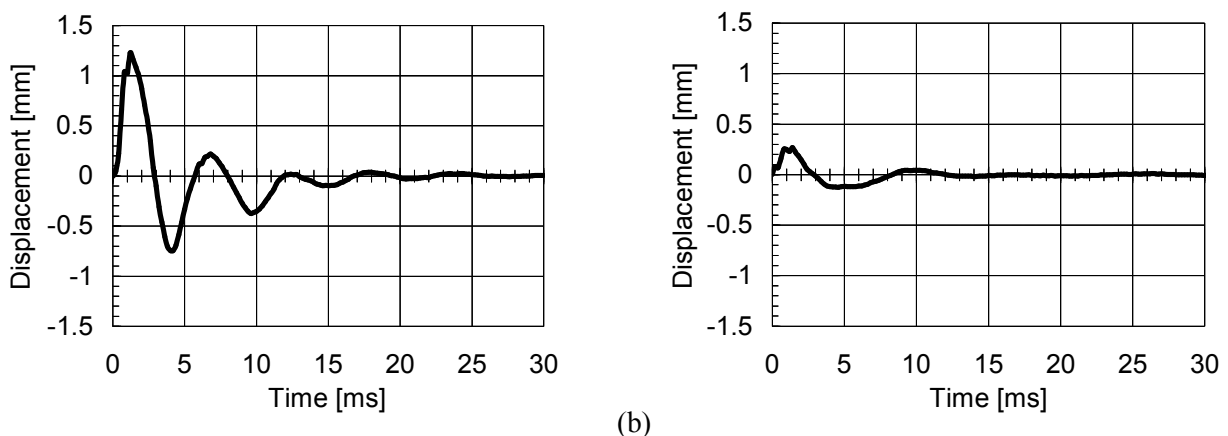


Figure 6. Typical particle displacements measured on the free surface associated with surface-breaking interface fracture, (a) on the hanging wall and (b) on the footwall (nonvertical case, time is zero when dynamic motion is detected for each diagram).

References

- [1] K. Aki, Seismic displacements near a fault. *J Geophys Res*, 73 (1968) 5359–5376.
- [2] K. Olsen, R. Madariaga, R. Archuleta, Three-dimensional dynamic simulation of the 1992 Landers earthquake. *Science*, 278 (1997) 834–838.
- [3] K. Uenishi, H. P. Rossmannith, A. E. Scheidegger, Rayleigh pulse – Dynamic triggering of fault slip. *Bull Seismol Soc Am*, 89 (1999) 1296–1312.
- [4] R. Madariaga, Radiation from a finite reverse fault in a half space. *Pure Appl Geophys*, 160 (2003) 555–577.
- [5] D. D. Oglesby, R. J. Archuleta, S. B. Nielsen, Earthquakes on dipping faults; the effects of broken symmetry. *Science*, 280 (1998) 1055–1059.
- [6] H. Kao, W.-P. Chen, The Chi-Chi earthquake sequence: Active, out-of-sequence thrust faulting in Taiwan. *Science*, 288 (2000) 2346–2349.
- [7] D. D. Oglesby, S. M. Day, Fault geometry and the dynamics of the 1999 Chi-Chi (Taiwan) earthquake. *Bull Seismol Soc Am*, 91 (2001) 1099–1111.
- [8] P. M. Davis, L. Knopoff, The dipping antiplane crack. *Geophys J Int*, 106 (1991) 581–585.
- [9] D. D. Oglesby, R. J. Archuleta, S. B. Nielsen, Dynamics of dip-slip faulting; Explorations in two dimensions. *J Geophys Res*, 105 (2000) 13,643–13,653.
- [10] R. Burridge, G. Halliday, Dynamic shear cracks with friction as models for shallow focus earthquakes. *Geophys J R Astron Soc*, 25 (1971) 261–283.
- [11] D. M. Boore, M. D. Zoback, Near-field motions from kinematic models of propagating faults. *Bull Seismol Soc Am*, 64 (1974) 555–570.
- [12] A. Niazi, An exact solution for a finite, two-dimensional moving dislocation in an elastic half space with applications to the San Fernando earthquake of 1971. *Bull Seismol Soc Am*, 65 (1975) 1797–1826.
- [13] M. Bouchon, K. Aki, Discrete wave number representation of seismic-source wavefields. *Bull Seismol Soc Am*, 67 (1977) 259–277.
- [14] B. Shi, J. N. Brune, Y. Zeng, A. Anoshahpoor, Dynamics of earthquake normal faulting: Two-dimensional lattice particle model. *Bull Seismol Soc Am*, 93 (2003) 1179–1197.
- [15] K. Uenishi, R. I. Madariaga, Surface breaking dip-slip fault: Its dynamics and generation of corner waves. *Eos Trans AGU*, 86 (2005) Fall Meet Suppl, Abstract S34A-03.
- [16] The accelerograms obtained by the K-NET (Kyoshin Net) have shown the same tendency. The K-NET by the National Research Institute for Earth Science and Disaster Prevention of Japan provides the strong-motion data on the Internet (<http://www.k-net.bosai.go.jp/>). At that time, the seismic data were systematically collected at 1,000 observatories deployed all over Japan, with the average interval of some 25 km. For the distributions of the hypocenters of the main and aftershocks, see e.g., A. Kato et al., Imaging the Source Region of the 2004 Mid-Niigata Prefecture Earthquake and the Evolution of a Seismogenic Thrust-Related Fold, *Geophys. Res. Lett.*, 32, doi:10.1029/2005GL022366, 2005.
- [17] S. Aoi, T. Kunugi, H. Fujiwara, Trampoline effect in extreme ground motion. *Science*, 322 (2008) 727–730.
- [18] The numerical simulations have been performed using the finite difference technique originally developed in K. Uenishi, H. P. Rossmannith, SWIFD Finite Difference Wave Simulator and User Manual, Vienna University of Technology, Vienna, 1995.
- [19] H. P. Rossmannith, K. Uenishi, N. Kouzniak, Blast wave propagation in rock mass – Part I: Monolithic medium. *Fragblast*, 1 (1997) 317–359.
- [20] K. Uenishi, H. P. Rossmannith, Blast wave propagation in rock mass – Part II: Layered media. *Fragblast*, 2 (1998) 39–77.
- [21] S. Ide, A. Baltay, G. C. Beroza, Shallow dynamic overshoot and energetic deep rupture in the 2011 M_w 9.0 Tohoku-oki earthquake. *Science*, 332 (2011) 1426–1429.